

# Haptic Implications of Tool Flexibility in Surgical Teleoperation

M. Tavakoli and Robert D. Howe

School of Engineering and Applied Sciences, Harvard University, Cambridge, MA 02138, USA

## Abstract

In space and surgical robotics applications, the desire is to use thin and lightweight manipulators and cable-driven end-effectors. This, however, introduces joint and/or link flexibility in the slave robot of a master-slave teleoperation system, reducing the effective stiffness of the slave and the transparency of teleoperation. Here, we analyze teleoperation transparency and stability under slave joint and link flexibility (tool flexibility) and evaluate the added benefits of using extra sensors at the tip of the flexible slave. One of the results of this paper is that tip velocity feedback can eliminate the display of joint or link flexibility to the user during a hard contact task.

## 1 Introduction

The use of thin, lightweight manipulators and cable-driven end-effectors in space and surgical robots results in flexibility in the link and/or joint of the manipulator. Flexibility can cause steady-state errors, transient errors and vibrations, and even instability in the system. In surgical robots, as the surgical tools become thinner for less invasiveness (e.g., < 3 mm in pediatric surgery), the effect of flexibility becomes more crippling because control laws based on the assumption of a rigid robot are no longer effective or accurate.

Previously, we have analyzed the effects of joint elasticity in the slave robot on the transparency of master-slave teleoperation [1]. In this paper, we address transparency and stability limitations resulting from link flexibility (tool flexibility) in a slave robot and examine what added benefits can tip sensors deliver.

An ideal 1-DOF teleoperation system, in which the master is rigid but the slave has a flexible tool that couples the actuator to the end-effector is shown in Figure 1, where  $I_m$ ,  $I_{sm}$ ,  $\tau_m$  and  $\tau_s$  are the master and the slave (excluding the flexible link) inertias and controller outputs, respectively. Also,  $-f_h$  and  $-f_e$  denote the forces exerted by the operator's hand on the master and by the environment on the slave, respectively. The hand-master position and the slave-environment position are denoted by  $\theta_h$  and  $\theta_e$  respectively, while  $\theta_s$  is used to show the slave's joint position, which is different from  $\theta_e$  due to the link flexibility. With a rigid link of length  $L$  and defining  $\omega_h = \dot{\theta}_h$  and  $\tau_h = Lf_h$ , the dynamics of the master are

$$I_m \dot{\omega}_h = \tau_m + \tau_h \quad (1)$$

## 2 Lumped Model of a 1-DOF Flexible-Link Slave

The exact dynamics of a flexible link are described by partial differential equations and have infinite dimensions. In the constrained assumed modes method, the deflection of the flexible link in Figure 1b is modeled as

$$\Delta y(x, t) = \sum_{i=1}^{\infty} F_i(x) q_i(t), \quad 0 \leq x \leq L \quad (2)$$

where  $q_i(t)$  are the assumed flexible modes and  $F_i(x)$  are the corresponding time-independent modes shape functions. Considering the first mode  $q_1(t)$ , which is capable of capturing the dominant frequency, Zhu et al. [2] presented a method for lumping the distributed mass of the flexible link to a point mass located at its tip followed by modeling the flexibility of the link by a weightless linear bending spring. Denoting the equivalent tip lumped mass by  $M_{se}$  and the equivalent bending spring stiffness by  $K_s$ , the resulting

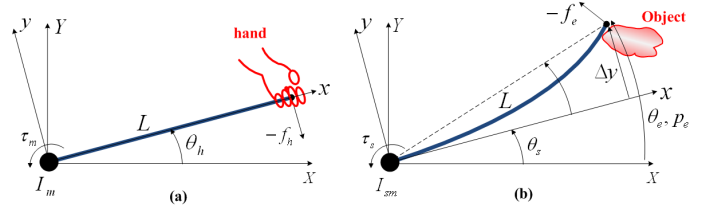


Figure 1: (a) The master; (b) the flexible-link slave.

lumped dynamic model of the flexible link in Figure 1b is

$$M_{se} \ddot{p}_e = -K_s \Delta y - f_e, \quad I_{sm} \ddot{\theta}_s = \tau_s + LK_s \Delta y \quad (3)$$

where  $p_e = L\theta_s + \Delta y$  is the arc approximation of the link tip position. Noting that  $\theta_e = p_e/L$  and defining  $\Delta\theta = \theta_s - \theta_e = -\Delta y/L$ ,  $I_{se} = M_{se}L^2$ ,  $k_s = K_sL^2$  and  $\tau_e = Lf_e$ , the lumped model of the flexible-link slave in Figure 1b is rewritten as

$$I_{se} \dot{\omega}_e = k_s \Delta\theta - \tau_e \quad (4)$$

$$I_{sm} \dot{\omega}_s = \tau_s - k_s \Delta\theta \quad (5)$$

where  $\omega_e = \dot{\theta}_e$  and  $\omega_s = \dot{\theta}_s$ . With  $\tau_s$  as the input, the system (4)-(5) has two poles at  $\pm j\omega_R = \pm j\sqrt{k_s(1/I_{sm} + 1/I_{se})}$  (resonance). For the controller output  $\tau_s$ , if  $\omega_s$  is the output, the system will have two zeros at  $\pm j\omega_0 = \pm j\sqrt{k_s/I_{se}}$  (anti-resonance). If  $\omega_e$  is taken as the output, however, the system will show no anti-resonance.

Interestingly, the lumped dynamics (4)-(5) of the flexible link are identical to the dynamics of the flexible joint shown in Figure 2 consisting of a motor with inertia  $I_{sm}$  and an end-effector with inertia  $I_{se}$  that are coupled via a shaft with a finite stiffness  $k_s$ . Therefore, the results of our previous study concerning teleoperation performance for different teleoperation control methods and sensor configurations with an elastic-joint slave are directly extended to the case of a flexible-link slave [1]. Additionally, we modify one of the previous teleoperation methods as described in the next section, and perform a simple absolute stability analysis on all of the methods.

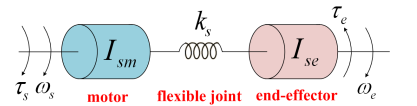


Figure 2: An elastic-joint slave robot.

## 3 Teleoperation Architectures vs. Sensor Configurations

Position error based (PEB) bilateral control uses no force sensor measurements and merely tries to minimize the difference between the master and the slave positions for providing haptic feedback to the user. Direct force reflection (DFR) bilateral control, however, employs a force sensor to measure slave-environment interactions for reflecting them to the user. In PEB and DFR methods, the master and slave controller outputs are

$$\tau_m = \dot{\omega}_{hd} + k_p(\omega_{hd} - \omega_h) + k_i \int (\omega_{hd} - \omega_h) dt, \quad \text{PEB} \quad (6)$$

$$\tau_m = -\tau_e, \quad \text{DFR} \quad (7)$$

$$\tau_s = \dot{\omega}_d + k_p(\omega_d - \omega) + k_i \int (\omega_d - \omega) dt, \quad \text{PEB/DFR} \quad (8)$$

where subscript  $d$  denotes the desired trajectories. Also, depending on whether the velocity sensor is placed on the motor or on the end-effector in Figure 2,  $\omega = \omega_s$  or  $\omega = \omega_e$ , respectively. Note

that, for simplicity, the master and slave controllers (PI-type on velocities and PD-type on positions) are chosen to be similar. As discussed in [1], we choose  $k_i = \beta^2 I_{sm}$  and  $k_p = 2\beta I_{sm}$  (for critical damping) where  $\beta > 0$  is a control gain affecting the placement of poles in the system. Assuming the PI controllers do not become saturated,  $\beta$  can be selected to be sufficiently large so that the dynamics contributed by the controller (involving  $(s + \beta)^2$ ) are much faster than those originating from the rest of the system including link flexibility. Therefore, assuming perfect position control of the slave (and the master in PEB control), we isolate the effect of flexibility in order to understand the fundamental limitations imposed by it on teleoperation transparency and the added benefits of using extra sensors at the tip of the slave.

Distinguishing several possible sensor configurations for a flexible-slave teleoperation system, in the following we examine the effect of slave robot flexibility for each control architecture on transparency. In an ideally transparent teleoperation system, through appropriate control actions  $\tau_m$  and  $\tau_s$ , we have  $\omega_h = \omega_e$  and  $\tau_h = \tau_e$ . We consider the following elements of hybrid, transmission and impedance matrices as our transparency indices:

- free-motion transmitted impedance  $h_{11} = F_h/\omega_h|_{F_e=0}$ ,
- free-motion position tracking index  $h_{21} = -\omega_e/\omega_h|_{F_e=0}$ ,
- hard-contact transmitted impedance index  $f_{12} = F_h/F_e|_{\omega_e=0}$ ,
- hard-contact transmitted impedance  $z_{11} = F_h/\omega_h|_{\omega_e=0}$ .

With the assumption of  $\beta \rightarrow \infty$ , the performance indices are listed for each of the following control architectures and sensor configurations in Table 1, in which  $R = I_{se}/I_{sm}$  and  $R' = I_m/I_{sm}$ .

**PEB control with feedback of  $\omega_s$ :** In this case,  $\omega_{hd} = \omega_s$  in (6) and  $\omega_d = \omega_h$  and  $\omega = \omega_s$  in (8).

**PEB control with feedback of  $\omega_e$ :** In this case,  $\omega_{hd} = \omega_e$  in (6) and  $\omega_d = \omega_h$  and  $\omega = \omega_e$  in (8).

**DFR control with feedback of  $\omega_s$  and  $\tau_e$ :** In this case,  $\omega = \omega_s$  in (8). It is possible to simply take  $\omega_d = \omega_h$  in (8) as was done for PEB control. However, since both  $\omega_s$  and  $\tau_e$  are available, it is possible to obtain  $\omega_d$  more accurately based on the open-loop system equation (4). Taking the time derivative of both sides of (4) gives  $I_{se}\dot{\omega}_e = k_s(\omega_s - \omega_e) - \tau_e$ . Since  $\omega_e = \omega_h$  is the performance goal, the desired trajectory for  $\omega_s$  becomes

$$\omega_d = \omega_h + (I_{se}/k_s)\dot{\omega}_h + \tau_e/k_s \quad (9)$$

**DFR control with feedback of  $\omega_e$  and  $\tau_e$ :** In this case,  $\omega_d = \omega_h$  and  $\omega = \omega_e$  in (8).

**DFR control with feedback of  $\omega_s$ ,  $\omega_e$  and  $\tau_e$ :** Since we have both  $\omega_s$  and  $\omega_e$  and we can also determine distinct desired trajectories for each of them due to the availability of  $\tau_e$  information, we employ a two-loop PI controller as proposed in [2] instead of (8):  $\tau_s = \sum_{\ell=1}^2 I_\ell(\dot{\omega}_{\ell d} + k_p(\omega_{\ell d} - \omega_\ell) + k_i \int (\omega_{\ell d} - \omega_\ell) dt)$ . Here,  $I_1 = I_{sm}$ ,  $\omega_1 = \omega_s$  and  $\omega_{1d}$  is obtained from (9). Also,  $I_2 = I_{se}$ ,  $\omega_2 = \omega_e$  and  $\omega_{2d} = \omega_h$ .

#### 4 Effects of Flexibility on Transparency and Stability

Table 1 assumes  $\beta$  is very large, yet the relative performance of different teleoperation architectures and sensor configurations can be inferred from it for the case that  $\beta$  is limited – see [1] for a full transparency comparison under limited  $\beta$ . Based on Table 1,

(1) From the first row ( $h_{11}$ ), while during PEB teleoperation the user will feel some residual impedance that depends on the slave's inertia and stiffness characteristics, during DFR teleoperation only the master inertia will be transmitted to the user. If acceleration feedforward is not provided during PEB, the user will feel the master inertia as well.

(2) From the second row ( $h_{21}$ ), with feedback of  $\omega_e$ , perfect position tracking can be attained in both PEB and DFR teleoperation regardless of the link flexibility. With feedback of  $\omega_s$ , perfect position tracking in DFR teleoperation is possible if the desired trajectory for  $\omega_s$  is determined from (9). Otherwise, position tracking with  $\omega_s$  feedback is satisfactory only at low frequencies.

Table 1: Performance indices of different teleoperation architectures and sensor configurations when  $\beta \rightarrow \infty$ . See [1] for limited  $\beta$  case.

Control	PEB	PEB	DFR	DFR	DFR	DFR	Ideal
Sensor	$\omega_s$	$\omega_e$	$\omega_s, \tau_e$	$\omega_s, \tau_e$ w/ (9)	$\omega_e, \tau_e$	$\omega_s, \omega_e, \tau_e$ w/ (9)	
$h_{11}$	$\frac{I_{se}s}{1+(\frac{s}{\omega_0})^2}$	$\frac{I_{se}s}{I_{sm}^2 s(\frac{s}{\omega_0})^2} +$	$I_{ms}$	$I_{ms}$	$I_{ms}$	$I_{ms}$	0
$h_{21}$	$\frac{-1}{1+(\frac{s}{\omega_0})^2}$	-1	$\frac{-1}{1+(\frac{s}{\omega_0})^2}$	-1	-1	-1	-1
$f_{12}$	1	$\frac{1}{1+\frac{1}{R}(\frac{s}{\omega_0})^2}$	$\frac{1}{1+\frac{R'}{R}(\frac{s}{\omega_0})^2}$	1	1	1	1
$z_{11}$	$\frac{k_s}{s}$	$\infty$	$I_{ms} + \frac{k_s}{s}$	$\infty$	$\infty$	$\infty$	$\infty$
Abs. stable	Yes	No	Yes for $\omega < \omega_0$	Yes	No	Yes	

(3) From the third row ( $1/f_{12}$ ), perfect force tracking can be attained in PEB teleoperation with feedback of  $\omega_s$  and in DFR teleoperation with feedback of  $\omega_e$  and/or with feedback of  $\omega_s$  if (9) is used for generating the desired trajectory of  $\omega_s$ . Otherwise, force tracking is satisfactory only in low frequencies.

(4) From the fourth row ( $z_{11}$ ), with knowledge of  $\omega_s$  only, the flexibility in the slave will be felt by the user during a hard contact task unless (9) is used for generating the desired trajectory of  $\omega_s$ . With feedback of  $\omega_e$ , however, hard surfaces can be displayed transparently to the user in both PEB and DFR teleoperation. This is consistent with the results of Christiansson and van der Helm [3].

(5) From the last row, obtained through examining Llewellyn's criterion for absolute stability (stability for any passive but otherwise arbitrary operator and environment terminations), teleoperation with feedback of  $\omega_e$  alone is not absolutely stable while it is absolutely stable with feedback of  $\omega_e$  and  $\omega_s$  (second last column in Table 1). This is consistent with Vukosavic and Stojic [4] that stability in servo drives similar to Figure 2 gets more difficult with load velocity feedback ( $\omega_e$ ) as the closed-loop system will encompass torsional resonance modes. Nonetheless, in practice friction has an stabilizing effect, and the presence of upper bounds on the dynamic ranges of the environment and operator impedances results in relaxed absolute stability conditions [5]. Lastly, note that the absolute stability results in Table 1 are valid only for very large  $\beta$  – stability analysis for a limited  $\beta$  is complex and remains as a future work.

#### 5 Conclusions

It was shown that velocity feedback from the tip of a flexible slave robot improves free-space position tracking performance and, in direct force reflection teleoperation, also improves hard-contact force tracking performance. Moreover, with tip velocity feedback, the flexibility in the slave will not be transmitted to the user during a hard contact task. Lastly, performance and stability benefits were witnessed when (9) is used for generating desired trajectories, however the trade-off is that obtaining noise-free torque and velocity information for differentiation in (9) is costly.

#### Acknowledgements

This research was supported by the NSF grant EEC-9731748 and an NSERC Postdoctoral Fellowship awarded to M. Tavakoli. The authors acknowledge helpful discussions with Allison M. Okamura (JHU) and Katherine J. Kuchenbecker (U Pennsylvania).

#### References

- [1] M. Tavakoli and R. D. Howe, "The effect of joint elasticity on bilateral teleoperation," in *Proceedings of 2007 International Conference on Intelligent Robots and Systems*, San Diego, CA, October 2007, pp. 1618–1623.
- [2] G. Zhu, S. S. Ge, and T. H. Lee, "Simulation studies of tip tracking control of a single-link flexible robot based on a lumped model," *Robotica*, vol. 17, no. 1, pp. 71–78, 1999.
- [3] G. A. V. Christiansson and F. C. T. van der Helm, "The low-stiffness teleoperator slave – a trade-off between stability and performance," *Int. J. Robotics Research*, vol. 26, no. 3, pp. 287–299, March 2007.
- [4] S. N. Vukosavic and M. R. Stojic, "Suppression of torsional oscillations in a high-performance servoservo drive," *IEEE Transactions on Industrial Electronics*, vol. 45, no. 1, pp. 108–117, February 1998.
- [5] K. Hashtrudi-Zaad and S. E. Salcudean, "Analysis of control architectures for teleoperation systems with impedance/admittance master and slave manipulators," *Int. J. Robotics Research*, vol. 20, no. 6, pp. 419–445, 2001.